

# UC Berkeley

## UC Berkeley Previously Published Works

### Title

Belowground allocation and dynamics of recently fixed plant carbon in a California annual grassland

### Permalink

<https://escholarship.org/uc/item/6xr1v5rm>

### Authors

Fossum, Christina

Estera-Molina, Katerina Y

Yuan, Mengting

et al.

### Publication Date

2022-02-01

### DOI

10.1016/j.soilbio.2021.108519

### Copyright Information

This work is made available under the terms of a Creative Commons Attribution License, available at <https://creativecommons.org/licenses/by/4.0/>

Peer reviewed



## Belowground allocation and dynamics of recently fixed plant carbon in a California annual grassland

Christina Fossum<sup>a</sup>, Katerina Y. Estera-Molina<sup>a</sup>, Mengting Yuan<sup>a</sup>, Donald J. Herman<sup>a</sup>,  
Ilexis Chu-Jacoby<sup>a</sup>, Peter S. Nico<sup>b</sup>, Keith D. Morrison<sup>c</sup>, Jennifer Pett-Ridge<sup>c,d</sup>,  
Mary K. Firestone<sup>a,\*</sup>

<sup>a</sup> Department of Environmental Science, Policy, and Management, University of California, Berkeley, CA, USA

<sup>b</sup> Earth Sciences Division, Lawrence Berkeley National Laboratory, Berkeley, CA, USA

<sup>c</sup> Physical and Life Sciences Directorate, Lawrence Livermore National Laboratory, Livermore, CA, USA

<sup>d</sup> Life and Environmental Sciences Department, University of California, Merced, CA, USA

### ARTICLE INFO

#### Keywords:

Soil organic matter (SOM)  
Annual grassland  
<sup>13</sup>C<sub>2</sub> pulse labeling  
SOM density Fractionation  
<sup>13</sup>C-NMR

### ABSTRACT

Plant roots and the organisms that surround them are a primary source for stabilized soil organic carbon (SOC). While grassland soils have a large capacity to store organic carbon (C), few field-based studies have quantified the amount of plant-fixed C that moves into soil and persists belowground over multiple years. Yet this characteristic of the soil C cycle is critical to C storage, soil water holding capacity, nutrient provisions, and the management of soil health. We tracked the fate of plant-fixed C following a five-day <sup>13</sup>C<sub>2</sub> labeling of a Northern California annual grassland, measuring C pools starting at the end of the labeling period, at three days, four weeks, six months, one year, and two years. Soil organic carbon was fractionated using a density-based approach to separate the free-light fraction (FLF), occluded-light fraction (OLF), and heavy fraction (HF). Using isotope ratio mass spectrometry, we measured <sup>13</sup>C enrichment and total C content for plant shoots, roots, soil, soil dissolved organic carbon (DOC), and the FLF, OLF, and HF. The chemical nature of C in the HF was further analyzed by solid state <sup>13</sup>C nuclear magnetic resonance (NMR) spectroscopy.

At the end of the labeling period, a substantial portion of the <sup>13</sup>C (40%) was already found belowground in roots, soil, and soil DOC. By 4 weeks, the highest isotope enrichment and 27% of the total amount of <sup>13</sup>C remaining in the system was associated with the mineral-rich HF. At the 6-month sampling—after the dry summer period during which plants senesced and died—the amount of label in the FLF increased to an amount similar to that in the HF. The FLF <sup>13</sup>C then declined substantially by 1 year and further decreased in the second year. By the end of the 2-year experiment, 67% of remaining label was in the HF, with 19% in the FLF and 14% in the OLF. While the <sup>13</sup>C content in the HF was stable over the final year, the chemical forms associated with the HF evolved with time. The relative proportion of aliphatic/alkyl C functional groups declined in the newly formed SOC over the 2 years in the field; simultaneously, aromatic and carbonyl/carboxylic C functional groups increased and the proportion of carbohydrate (O-alkyl C) groups remained relatively constant.

Our results indicate that plant-fixed C moved into soil within days of its fixation and was associated with the soil mineral fraction within weeks. While most of the annual plant C input in these grasslands cycles rapidly (<2-year timescale), a sizeable proportion (about 23% of the <sup>13</sup>C present at day 0) persisted in the soil for longer than 2 years. While decadal studies would allow improved assessment of the long-term stabilization of newly fixed plant C, our 2-year field study reveals surprisingly rapid movement of plant C into the HF of soil, followed by subsequent evolution of the chemical forms of organic C in the HF.

### 1. Introduction

California annual grasslands occupy over 2.9 million ha (George

2020) and may be a more resilient and effective C sink than California's fire-prone forests (Dass et al., 2018). According to a recent meta-analysis, grassland soils also have an increased capacity to store

\* Corresponding author. Department of Environmental Science, Policy, and Management, 134 Mulford Hall, University of California, Berkeley, CA 94720, USA.  
E-mail address: [mkfstone@berkeley.edu](mailto:mkfstone@berkeley.edu) (M.K. Firestone).

soil C in the face of increasing atmospheric CO<sub>2</sub> concentrations (Terrier-Moreno et al., 2020). As such, these ecosystems have become an attractive target for California state policy initiatives aimed at mitigating atmospheric CO<sub>2</sub> levels through soil C sequestration (Biggs and Huntsinger, 2021; Baker et al., 2019). However, our mechanistic understanding of soil C cycling, the fate and persistence of plant C inputs belowground, and how annual grasslands can act as a viable C sink remains incomplete (Bradford et al., 2019). To effectively manage C stocks, further research is required to better understand the ecological parameters that regulate soil C cycling in these globally significant ecosystems.

Belowground C dynamics in California annual grasslands reflect the annual plant life cycle (Eviner and Firestone, 2007). These grassland's plant communities are dominated by annual grasses and forbs, species whose reproductive strategies are well-adapted to a Mediterranean climate where seasonal moisture limitations regulate nutrient cycling. This climate is characterized by cool wet winters and a warm summer period with no rainfall, a defining feature of which is the misalignment of two critical conditions for plant growth: rainfall and solar energy. Moisture limits plant growth in the summers, and sunlight and temperature limit plant growth in the winters (Bartolome et al., 2007; Eviner and Firestone, 2007). The plant life cycle begins with the first germinating rainfall in the autumn, proceeds slowly through the winter due to sunlight and temperature limitations, peaks in the spring when both soil moisture and sunlight are usually optimized, and ends with plant senescence that coincides with declining soil moisture and the onset of the summer dry period (Eviner, 2001; Eviner and Firestone, 2007). Throughout the winter/spring growing season, C enters the soil primarily via the constant 'drip' of plant root exudation (Sokol and Bradford, 2019; Pett-Ridge et al., 2021); over the summer dry period, plant senescence and subsequent litter input, coupled with low-moisture conditions drives the transient accumulation of litter; in the autumn at the onset of the rainy season, a large portion of accumulated C is rapidly released as CO<sub>2</sub> in a decomposition 'pulse' (Blankinship and Schimel, 2018; Barnard et al., 2020). While not fully understood, the wet-dry cycles characteristic of California annual grasslands may be important drivers of SOM persistence and may be susceptible to future climate conditions that either amplify or minimize their stabilizing or destabilizing effects (Bailey et al., 2019).

Soil organic C is often considered and modelled in terms of distinct SOM pools: either associated with minerals, occluded within micro-aggregates, or "free" (not subject to either chemical or physical protection) (Poelplau et al., 2018; Lavalley et al., 2019). Recent studies have shown that labile C substrates can play an important role in SOM formation and stabilization in both physically (occluded) and chemically (mineral-associated) pools (Cotrufo et al., 2015; Totsche et al., 2017; Villarino et al., 2021); plant litter is presumed the dominant component of FLF material. The mineral-associated pool or "heavy fraction" is of particular interest for SOC persistence; C in this fraction can represent one of the oldest distinct pools (Torn et al., 1997) and may be stabilized via mineral sorption and co-precipitation mechanisms (Kögel-Knabner et al., 2008). This fraction of SOM, commonly termed MAOM (mineral-associated organic matter) (Cotrufo et al., 2019), is largely of microbial origin in grasslands (Angst et al., 2021) and is thought to be derived from relatively labile C substrates (Clemente et al., 2011; Cotrufo et al., 2013; Villarino et al., 2021).

Tracking both the source and persistence of SOC associated with different soil C pools has typically been accomplished through isotope amendment studies, where leaf or root litter (Hicks Pries et al., 2017; Kandeler et al., 2019), or known root exudate compounds (Geyer et al., 2020; Keiluweit et al., 2015) are added to a soil and traced into soil C pools over time. These studies have shown differential persistence of distinct substrates, in different soil horizons, under disparate management regimes. However, the longevity estimates of amendment studies may be inaccurate due to the artificial nature of the substrate introduction procedure. By contrast, *in situ* tracer experiments, while less

**Table 1**

**Site characteristics and soil physicochemical properties at the Hopland Research and Extension Center (HREC), Hopland, CA.** Location and soil pedology information are from the Natural Resources Conservation Service (NRCS) Web Soil Survey. Elevation and climate characteristics were described by HREC. Soil texture and CEC were determined at the UC Davis analytical lab. Mineralogy was determined at LLNL by X-ray diffraction. Aggregate stability, defined as % water-stable aggregates, was measured on soil collected in March 2018. SOC, TN, C/N, pH, and moisture were collected at the 4-week sampling time (Spring 2018). Values are means ± one standard deviation.

Characteristic	Field Site: HREC
<b>Location</b>	39°00'14.6"N 123°05'09.1"W
<b>Elevation (m)</b>	244
<b>Mean Annual Temperature (°C)</b>	14
<b>Mean Annual Precipitation (cm)</b>	94
<b>Soil type</b>	Typic Haploxeralf
<b>Series name</b>	Squawrock-Witherell Complex
<b>Bulk density</b>	1.457 g/cm <sup>3</sup>
<b>Aggregate stability</b>	39 ± 7
<b>Cation Exchange Capacity (cmol kg<sup>-1</sup>)</b>	18.75
<b>Soil organic carbon (mg (g soil)<sup>-1</sup>) (Spring)</b>	13.1 ± 1.7
<b>Soil organic carbon (mg (g soil)<sup>-1</sup>) (Fall)</b>	15.1 ± 2.0
<b>Total Nitrogen (mg (g soil)<sup>-1</sup>) (Spring)</b>	1.4 ± .1
<b>Total Nitrogen (mg (g soil)<sup>-1</sup>) (Fall)</b>	1.5 ± .2
<b>C/N (Spring)</b>	9.8 ± .4
<b>C/N (Fall)</b>	10.2 ± .5
<b>Texture</b>	48, 35, 17
<b>Clays (30%)</b>	Muscovite (17.8%) Chlorite (11.8%) Kaolinite (0.7%)
<b>Non-clays (70%)</b>	Quartz (47.3%) Plagioclase (22.4%)
<b>pH (Spring)</b>	5.9 ± .1
<b>pH (Fall)</b>	7.3 ± .1
<b>Soil Moisture % (Spring)</b>	14.3 ± 2.6
<b>Soil Moisture % (Fall)</b>	1.9 ± .3

common, are conceptually more realistic (Heckman et al., 2021; Pett-Ridge and Firestone, 2017). In an *in situ* tracer study, isotope (<sup>13</sup>C or <sup>14</sup>C) is introduced to the plant-microbe-soil continuum via photosynthate, then to exudates and growing roots. As these roots grow and then decay, they are enveloped by a large biomass of saprotrophic microorganisms and extracellular polymeric substances. This concentration of decomposition catalysts rapidly processes plant-derived C and produces diverse organic materials that may be subsequently respired away, or stabilized (Pett-Ridge et al., 2021).

In this study, we used an *in situ* <sup>13</sup>C tracer approach to follow plant-fixed C entering the soil and moving into various SOM pools and tracked its form and transformations over the course of two full annual (wet-dry) cycles. Because most soils are not rapidly accruing SOC, we expected the amount of <sup>13</sup>C remaining to decline rapidly, possibly reaching natural abundance by 2 years; we expected the location and forms of the "new" C to become indistinguishable from the resident SOC. To test these expectations, we introduced the stable isotope <sup>13</sup>C to the system as photosynthetically-fixed C, via a 5-day <sup>13</sup>CO<sub>2</sub> field labeling of a California annual grassland plant community. To quantify the dynamics of the added <sup>13</sup>C tracer in aboveground plant biomass, plant roots, soil, and various SOM pools, we sampled biomass and soil at multiple timepoints following the field labeling (immediately after, 3 days, 4 weeks, 6 months, 1 year, and 2 years), and physically fractionated soil samples with a sodium polytungstate density gradient-based procedure. We isolated 3 soil density fractions: (HF) the heavy fraction (mineral-associated SOM, MAOM), (OLF) the occluded-light fraction (micro-aggregate occluded SOM), and (FLF) the free-light fraction (accessible SOM debris) (Golchin et al., 1994; Sollins et al., 2009). We further characterized the chemistry of the HF <sup>13</sup>C using solid-state CPMAS <sup>13</sup>C NMR spectroscopy, to better understand both the composition of C newly incorporated into this fraction, as well as the influence of new inputs on

the total mineral-associated C pool. By combining  $^{13}\text{C}$  labeling, soil density fractionation, and solid-state  $^{13}\text{C}$  NMR, we sought to quantify the flow and fate of newly-fixed C entering this annual grassland soil, characterize its form and temporal dynamics, and thus better understand the mechanisms of C loss and persistence in this annual grassland soil.

## 2. Methods

### 2.1. Field site description

Field work was conducted at the University of California (UC) Hopland Research and Extension Center (HREC), in southwestern Mendocino County, CA (39° 00' 14.6" N, 123° 05' 09.1" W); the field station exists on territory originally home to the indigenous Pomo Nation. The region has a Mediterranean climate, with cool, wet winters and hot, dry summers. The vegetation community is dominated by naturalized annual grass and forb species including *Avena* spp., *Festuca* spp., *Erodium* spp., and *Bromus* spp. (Bartolome et al., 2007). Today, HREC is operated by the UC system as a working sheep ranch. Our field plots have been fenced off from grazing for >20 years. The soil at our field site belongs to the Squawrock-Witherell complex, a loamy-skeletal, mixed, superactive, thermic Typic Haploxeralf. The underlying parent material is colluvium derived from sandstone (Soil Survey Staff, 2020). Our measurements indicate that the dominant clays are muscovite, chlorite, and kaolinite; dominant non-clay minerals are quartz and plagioclase (Table 1). Annual net primary production for this site was estimated to be 856 g C m<sup>-2</sup> from 2018 to 2020 by a moderate resolution imaging spectroradiometer (MODIS)-based model (Zhu et al., 2018).

### 2.2. Experimental design

Samples collected for this study are a subset from a larger  $^{13}\text{CO}_2$  labeling and precipitation manipulation field experiment. In the spring of 2017, sixteen 3.24 m<sup>2</sup> plots were established, each delineated by a 1 m deep plastic liner to limit soil water equilibration with surrounding soils, and each containing six 40 cm diameter circular subplots. Circular subplots were surrounded by a 15 cm deep PVC "collar" designed to be fitted with an above-ground cylindrical chamber for labelling plants with either  $^{12}\text{C}$  or  $^{13}\text{C}$ -CO<sub>2</sub> (Supplemental Fig. 1A). Each circular subplot was subdivided into four 15 cm deep sections via plexiglass dividers; this "wedge" design allowed us to destructively harvest  $^{13}\text{CO}_2$  labeled soil and biomass from a single circular subplot at multiple timepoints following a labeling event (Supplemental Fig. 1B). Removable shelters were installed above all plots so that precipitation could be carefully controlled.

Experimental plots were labeled with  $^{12}\text{CO}_2$  or  $^{13}\text{CO}_2$  (99 atm %, Cambridge Isotopes) for 5 days from February 11–15, 2018, consistent with the expected maximum root development phase of *Avena* spp. plant growth (the plots were seeded the prior year to encourage a *Avena* spp. dominated community). CO<sub>2</sub> levels during the pulse labeling event were monitored with a Picarro G2200-I analyzer (for  $^{13}\text{C}$ ) and infrared gas analyzer (IRGA) (for  $^{12}\text{C}$ ). For the labeling, well-sealed cylindrical chambers made of PAR transmissive PVC film were fitted over two circular subplots per plot (Supplemental Fig. 1A). Plants within these chambers were exposed to either  $^{12}\text{CO}_2$  or an isotopically labeled analog,  $^{13}\text{CO}_2$ , resulting in 16  $^{12}\text{CO}_2$ -labeled 'control' subplots and 16  $^{13}\text{CO}_2$ -labeled subplots. The headspace CO<sub>2</sub> concentrations within the chambers were maintained between 400 and 1500 ppm during the daytime, and chambers were vented to equilibrate with atmospheric CO<sub>2</sub> conditions at dawn each day. Headspace  $^{13}\text{C}$  enrichment of  $^{13}\text{CO}_2$ -labeled subplots was maintained between 30 and 75 atom%. Plots were exposed to two different precipitation regimes; however, we did not detect a statistically significant ( $p < 0.05$ ) precipitation treatment effect on any soil or plant characteristics measured in this study; thus, replicates from these treatments were pooled for final analyses such that  $n =$

8 for most of the analyses presented.

### 2.3. Field sampling of $^{13}\text{C}$ labeled biomass and soil

Soil was sampled at six times following the  $^{13}\text{CO}_2$  labeling event: (1) immediately after the 5-day labeling period (0-day), (2) three days later (3-day), (3) four weeks after the first sampling (4-week), (4) six months after the first sampling (6-month), (5) one year after the first sampling (1-year), and (6) two years after the first sampling (2-year). The first three sampling times happened in the Spring of 2018. The 6-month, 1-year and 2-year sampling times were in Fall 2018, Spring 2019, and Spring 2020, respectively. At each sampling time, we collected 8 replicate samples from each experimental treatment ( $^{12}\text{C}$ -labeled,  $^{13}\text{C}$ -labeled).

Root and shoot biomass samples were collected at three times following the  $^{13}\text{CO}_2$  pulse labeling: (1) at 0-day, when we expected the maximum  $^{13}\text{C}$ -labeled shoot biomass, (2) at 3 days, to allow further migration of photosynthetically fixed  $^{13}\text{C}$  into the roots, the surrounding soil microbial community, and the soil environment, and (3) at 4 weeks, by which time we expected a measurable fraction of  $^{13}\text{C}$  label to have been translocated to root biomass and the surrounding soil. Shoot biomass was collected by clipping all live aboveground plant tissue from a single subplot "wedge", and then scaling up to g m<sup>-2</sup>. Root biomass was collected from three 2.45 cm cores that were installed in each wedge at the time of harvest and scaling up to the full wedge volume (1/4 × 40 cm subplot × 15 cm depth), and then g m<sup>-2</sup>. Prior to the 6-month sampling time, aboveground litter remaining from the 2017–2018 growing season was removed from the plots.

At each of the first four sampling times, we destructively harvested a quarter of a labeled subplot which resulted in 16 "wedges" of soil per sampling time. From each wedge, visible roots were removed, soil was homogenized, 500 g sub-samples were collected, air-dried, and stored at ambient temperature for further analysis. Separate 100 g fresh soil sub-samples were collected and stored briefly at 4 °C until processing for soil pH, DOC, and soil moisture. At each of the final two sampling times (1-year and 2-year), we collected two cores per wedge (2.54 cm diameter × 15 cm deep) rather than the whole wedge to preserve the remaining soil for future experiments. In these two cores we removed roots and homogenized the soil (~300 g) as above, then air dried and stored the soil for further analyses.

Altogether, eight  $^{13}\text{C}$ -labeled and eight  $^{12}\text{C}$ -labeled shoot, root, and soil samples were collected at 0 day, 3 days, and 4 weeks after labeling. Senescence of  $^{13}\text{C}$ -labeled plants occurred over the summer of 2018, between the 4-week and 6-month sampling times. Therefore, for the remaining sampling times (6-month, 1-year, and 2-year), only soil samples were collected (eight  $^{13}\text{C}$ -labeled and eight  $^{12}\text{C}$ -labeled).

### 2.4. Processing and diagnostic analyses of soil, root, and shoot biomass

Aboveground biomass dry weight was determined by drying harvested biomass at 65 °C until a stable dried weight was achieved. Root biomass dry weight was determined by hand picking live roots from collected root biomass cores, washing, and drying at 65 °C until dried weights stabilized. Dry root biomass per wedge was then calculated by scaling the dried root weights to the volume of the wedge.

Soil pH was determined in a 1:1 ratio of fresh homogenized soil to 0.01 M CaCl<sub>2</sub>. Soil gravimetric water content was assessed by drying a 10 g subsample of fresh homogenized soil at 105 °C until dried weights stabilized, then calculating percent water. Root free soil from the dried gravimetric water samples was used for bulk soil  $^{13}\text{C}$  IRMS analysis. DOC was extracted from 5 g fresh soil with 20 ml 0.5 M K<sub>2</sub>SO<sub>4</sub>. DOC and  $^{13}\text{C}$ -DOC was assessed by the Yale Analytical and Stable Isotope Center (YASIC) via a wet oxidation method (Lang et al., 2012). All remaining analyses were conducted on homogenized air-dry soil. Soil texture analysis was conducted by the UC Davis Analytical Lab via the hydrometer method (Sheldrick and Wang, 1993). Aggregate stability was

conducted using a wet sieving method previously adapted by Sher et al. (2020), using a custom wet-sieve apparatus (Singer et al., 1992; Sher et al., 2020).

## 2.5. Soil quantitative X-ray diffraction (XRD) analysis

Soil mineralogy was determined at Lawrence Livermore National Lab (Zhou et al., 2018). Soil samples were dried, crushed and passed through a 500  $\mu\text{m}$  sieve. Then 3 g of soil was ground with 15 mL of methanol in a McCrone mill with corundum grinding elements for 5 min. The sample was transferred to a plastic tray, air dried and homogenized on a vortex mixer with 10 mm plastic beads for 3 min (Bakker et al., 2018). The homogenized soil powders were then side loaded into XRD sample holders and analyzed on a Bruker D8 advance XRD, scanning from 3 to 65° 2 $\theta$  with a step size of 0.011° at a rate of 5 s per step. Quantitative analysis was done using BGMN Rietveld refinement and the Profex interface software (Doebelin and Kleeberg, 2015). The XRD patterns were refined to fit crystal unit cell parameters, size, site occupancy and preferred orientation.

## 2.6. Soil density fractionation

Soil density fractionation was performed on samples collected at 4-week, 6-month, 1-year, and 2-year sampling times. Air-dried soil was sieved to 2 mm before being fractionated into three discrete pools of SOM using a sodium polytungstate (SPT) density gradient: free-light fraction (FLF,  $\rho < 1.75 \text{ g cm}^{-3}$ ), occluded-light fraction (OLF,  $\rho < 1.75 \text{ g cm}^{-3}$ ), and mineral-associated or heavy fraction (HF,  $\rho > 1.75 \text{ g cm}^{-3}$ ). The density of  $1.75 \text{ g cm}^{-3}$  was chosen due to the similarities in mineralogy and soil physical characteristics between our sampling site and the site sampled in Neurath et al. (2021), which used this same SPT approach.

The method for density fractionation used in our study was adapted from Hicks Hicks Pries et al. (2017), previously adapted from Strickland and Sollins (1987). For each sample, 50 mL of sodium polytungstate (SPT-0, Geoliquids) prepared to a density of  $1.75 \text{ g cm}^{-3}$  was added to a 250 mL centrifuge tube containing 20 g of air-dried soil. The mixture was inverted by hand to ensure all soil came into contact with the SPT; soil remaining on the lid and sides was rinsed with an additional 50 mL of SPT. The SPT-soil solutions were allowed to settle for 1 h, then centrifuged for 1 h at 3700 RCF in a swinging bucket rotor (Beckman Avant J-20 Floor Centrifuge with JS-5.3 rotor). Following centrifugation, samples were allowed to settle until no particles remained suspended. Particles floating on top of the SPT solution were defined as the FLF and were isolated by aspirating onto a 0.7  $\mu\text{m}$  glass microfiber filter (Wattman), and rinsed with MilliQ water to remove residual SPT. Then, the FLF filters were transferred into drying tins in a 55 °C oven until any standing water had evaporated.

To release the OLF from microaggregates, the remainder of the soil-SPT mixture was mixed with a benchtop mixer for 1 min, followed by sonication for 90 s. As above, the soil was then rinsed, allowed to settle, centrifuged for 1 h, and the floating fraction was isolated via aspiration and dried.

The remaining sediment ( $\rho > 1.75 \text{ g cm}^{-3}$ ) was defined as the HF. This fraction was rinsed with 150 mL Milli-Q H<sub>2</sub>O, vigorously shaken by hand, centrifuged for 20 min, followed by aspiration and disposal of the supernatant. This was repeated 5 times, or until the density of the supernatant was  $\sim 1 \text{ g cm}^{-3}$ . The HF was transferred into drying tins and dried at 55 °C. Once standing water had evaporated, all three fractions were transferred to a 105 °C oven for 48 h. Oven-dried samples were cooled in a desiccator before being weighed, ground with a mortar and pestle, and stored in glass vials.

## 2.7. Isotopic and elemental analysis

Prior to elemental analysis, samples were ground to a fine powder

and weighed into aluminum tins, with sample weight proportional to expected C content (4 mg for the FLF, 2 mg for the OLF, 50 mg for the HF and bulk soil, 0.35 mg for shoot biomass, and 0.30 mg for root biomass samples). Bulk and density fractionated soil were ground using a mortar and pestle, aboveground biomass was ground in a coffee grinder, and root biomass was ground by hand. Total C, N, and <sup>13</sup>C enrichment were measured via total combustion using an elemental analyzer coupled with a continuous flow Isotope Ratio Mass Spectrometer (IRMS) at the Stable Isotope Facility at the University of California, Davis (AOAC Official Method 972.43).

## 2.8. <sup>13</sup>C-NMR

Subsamples of HF material were analyzed by <sup>13</sup>C-NMR to assess broad chemical composition of mineral-associated organic matter. Solid-state <sup>13</sup>C cross polarization magic angle spinning (CPMAS) spectroscopy was run on one <sup>13</sup>C-labeled HF sub-sample from the 4-week, 1-year, and 2-year sampling times, as well as one <sup>12</sup>C-labeled control HF subsample from the 4-week timepoint as a control comparison. These four spectra were acquired using a 4 mm log-gamma CPMAS probe on a 500 MHz Bruker Avance 1 NMR spectrometer at the UC Davis NMR facility. Samples were spun at 10 kHz with an acquisition time of 41 ms. Scan number ranged from 75,000 to 102,400. Glycine (176 ppm) was used as the external reference. Using Bruker's Topspin software, data were zero filled to 8k; an exponential function with 500 Hz of line broadening was used for signal processing, with zero order phase correction, followed by manual baseline correction.

Broad C functional groups were defined based on the following chemical shift regions: aliphatic/alkyl C (0–45 ppm), O-alkyl C (45–110 ppm), aromatic and aryl C (110–162 ppm), and carbonyl/carboxylic C (162–190 ppm) (Helfrich et al., 2006). Integration of chemical shift regions was conducted using Topspin 3 software to calculate relative contribution of different functional group regions to total peak area (0–190 ppm).

## 2.9. Calculation of ecosystem <sup>13</sup>C assimilation

We define ecosystem assimilated <sup>13</sup>C as that quantifiable in (1) aboveground (plant biomass) and (2) belowground (soil + root biomass) pools, i.e. net <sup>13</sup>C gain rather than gross ecosystem exchange. Ecosystem <sup>13</sup>C assimilation was calculated by converting the <sup>13</sup>C concentration of each pool (aboveground biomass, root biomass, soil in mg/g) to quantity ( $\text{g}^{13}\text{C m}^{-2}$  over a 15 cm sampling depth) and then summing. For simplicity, the sum of <sup>13</sup>C recovered in aboveground biomass plus soil and root biomass immediately after the pulse labeling period (0-day) was interpreted to equal 100% of assimilated <sup>13</sup>C. The percentage of assimilated <sup>13</sup>C remaining at each subsequent sampling timepoint was then calculated relative to this original amount. We note that at the 6-month, 1-year and 2-year sampling times, <sup>13</sup>C-labeled aboveground biomass and roots had senesced and the aboveground pool was not measured, and roots were not physically separated from the soil as had been done for the 0-day and 4-week timepoints. Average <sup>13</sup>C recovery based on summing the FLF + OLF + HF was approximately 72% that of the bulk soil, which is within the range for density fractionated soil C recovery values cited in the literature (Crow et al., 2007; Cusack et al., 2018). For clarity, we assumed that the measured distribution of <sup>13</sup>C in the FLF, OLF, and HF fractions represented the distribution of the total isotope pool in soil after the 4-week sampling.

## 2.10. Statistical analyses

The differences in total C, total N, C/N ratio, <sup>13</sup>C content and <sup>13</sup>C enrichment among sampling times and density fractions were tested using a two-way ANOVA (model: response variable ~ sampling time\* density fraction), followed by Tukey's HSD post-hoc tests with the R package 'agricolae' (Mendiburu, 2015). The effects of sampling time on

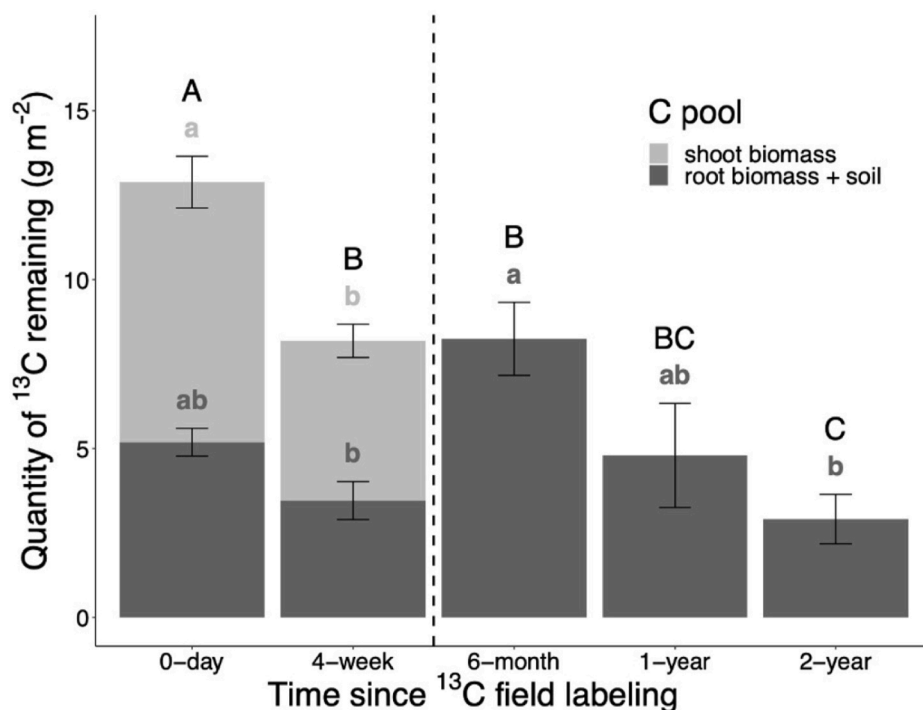


**Fig. 1.** Ecosystem <sup>13</sup>C assimilation following a 5-day *in situ* <sup>13</sup>CO<sub>2</sub> labelling experiment in an annual grassland near Hopland, CA. Bars represent total excess <sup>13</sup>C measured in shoot biomass and root biomass + soil. The 0-day sampling occurred immediately after the 5-day <sup>13</sup>CO<sub>2</sub> labeling. Vertical black dashed line between the 4-week and 6-month sampling time marks plant senescence at the end of the spring growing season; there was no shoot biomass beyond that point, and previously living root <sup>13</sup>C biomass had become part of the soil <sup>13</sup>C. Different lowercase letters indicate significant differences ( $p < 0.05$ ) between sampling time within a given C pool (in the same colors as the bars). Different capital letters indicate significant difference of total remaining <sup>13</sup>C between sampling time. Error bars represent 1 standard error ( $n = 8$ ).

**Table 2**

**Characteristics of soil density fractions collected at four sampling points after a 5-day *in situ* <sup>13</sup>CO<sub>2</sub> labelling.** Dry mass (g) values represent quantities of recovered materials in each density fraction from the starting soil samples (~20 g). Means are shown ± one standard deviation. Different letters represent significance differences among fractions and sampling times at  $p < 0.05$ . Total C and total <sup>13</sup>C results are visualized in Fig. 2.

Sampling time	Density Fraction	Total C (mg g <sup>-1</sup> )	Total N (mg g <sup>-1</sup> )	C/N Ratio	δ <sup>13</sup> C	Total <sup>13</sup> C (ug g <sup>-1</sup> )	Dry mass (g)
Spring 2018	FLF	1.58 ± .48 b	.08 ± .03 b	19.88 ± 2.97 c	30.14 ± 26.60	0.85 ± 0.38 b	.12 ± .03
	OLF	2.12 ± .58 b	.12 ± .03 b	17.51 ± 1.08 b	4.14 ± 26.73	0.82 ± 0.78 b	.11 ± .03
	HF	7.10 ± 1.60 a	.86 ± .14 a	8.20 ± .58 a	21.95 ± 14.36	3.71 ± 1.29 a	19.47 ± .18
Fall 2018	FLF	1.94 ± .65 b	.09 ± .03 b	20.65 ± 2.75 c	237.79 ± 74.35	5.25 ± 2.77 a	.18 ± .04
	OLF	2.26 ± .60 b	.13 ± .04 b	17.47 ± 0.98 b	24.61 ± 16.25	1.22 ± 0.43 b	.12 ± .03
	HF	7.77 ± 1.57 a	.91 ± .15 a	8.50 ± .45 a	30.69 ± 17.06	5.03 ± 1.41 a	19.38 ± .20
Spring 2019	FLF	1.62 ± .37 b	.09 ± .02 b	19.13 ± 1.76 c	78.31 ± 57.20	1.97 ± 1.26 ab	.14 ± .04
	OLF	2.39 ± .64 b	.14 ± .04 b	17.26 ± .87 b	8.04 ± 17.68	1.09 ± 0.65 b	.11 ± .04
	HF	7.14 ± 1.57 a	.84 ± .13 a	8.47 ± .75 a	24.46 ± 20.47	3.92 ± 1.88 a	19.41 ± .18
Spring 2020	FLF	0.91 ± .23 c	.05 ± .01 b	18.75 ± 2.10 b	51.33 ± 64.35	0.77 ± 0.58 b	.09 ± .03
	OLF	1.81 ± .68 b	.10 ± .04 b	17.79 ± .76 b	0.44 ± 16.62	0.57 ± 0.57 b	.10 ± .04
	HF	6.30 ± 1.09 a	.79 ± .11 a	7.99 ± .57 a	15.82 ± 19.31	2.91 ± 1.61 a	19.57 ± .15

the aboveground <sup>13</sup>C, belowground <sup>13</sup>C, shoot enrichment, root enrichment, and DOC enrichment were tested using one-way ANOVA (model: response variable ~ sampling time), followed by Tukey's HSD test. Data were visualized using the R package 'ggplot2' (Wickham, 2016).

### 3. Results

#### 3.1. Ecosystem <sup>13</sup>C incorporation

Immediately following the <sup>13</sup>CO<sub>2</sub> labeling, all four C pools (soil, shoot and root biomass, DOC) were significantly <sup>13</sup>C enriched (Fig. 1, Supplemental Fig. 2). We defined the total amount of <sup>13</sup>C present at 0-day to be 100% and calculated pools thereafter relative to this starting amount. During the 5-day labeling, over 12 g <sup>13</sup>C m<sup>-2</sup> derived from plant photosynthate accumulated in these C pools, accounting for roughly 0.2% of total ecosystem C content (aboveground biomass, root biomass, and soil in the 0–15 cm depth horizon). By 4 weeks, <sup>13</sup>C content of the shoot biomass pool had declined to 61.7% of its initial amount ( $p = 0.015$ ) (Fig. 1). Transfer of plant-fixed <sup>13</sup>C to belowground pools was

immediate, accounting for 40% of total ecosystem <sup>13</sup>C immediately after the labeling. Belowground <sup>13</sup>C content reached a maximum at 6 months post-labeling. Between the 6-month, 1-year, and 2-year sampling times, assimilated <sup>13</sup>C in the soil decreased stepwise: 64% of the original <sup>13</sup>C remained at 6 months, 37% at 1 year, and 23% at 2 years (Fig. 1).

Samples collected at 0, 3 days, and 4 weeks were used to assess short-term dynamics of root and DOC enrichment. While the enrichment of roots tended to increase from 0 day to 4 months and the enrichment of DOC decreased over the same period; none of these short-term changes were statistically significant (Supplemental Fig. 2).

#### 3.2. Soil density fractions

We used density fractionation to assess changes in the quantity and quality of newly-fixed plant-derived C in soil samples collected at 4 weeks, 6 months, 1 year, and 2 years after field labeling. The HF accounted for roughly 99% of the total recovered soil mass (average between all sample times) (Table 2) and contained the largest fraction of C, accounting for 66% of the total, while the OLF accounted for 20%, and FLF 14% (Fig. 2). The distribution of total N followed a similar

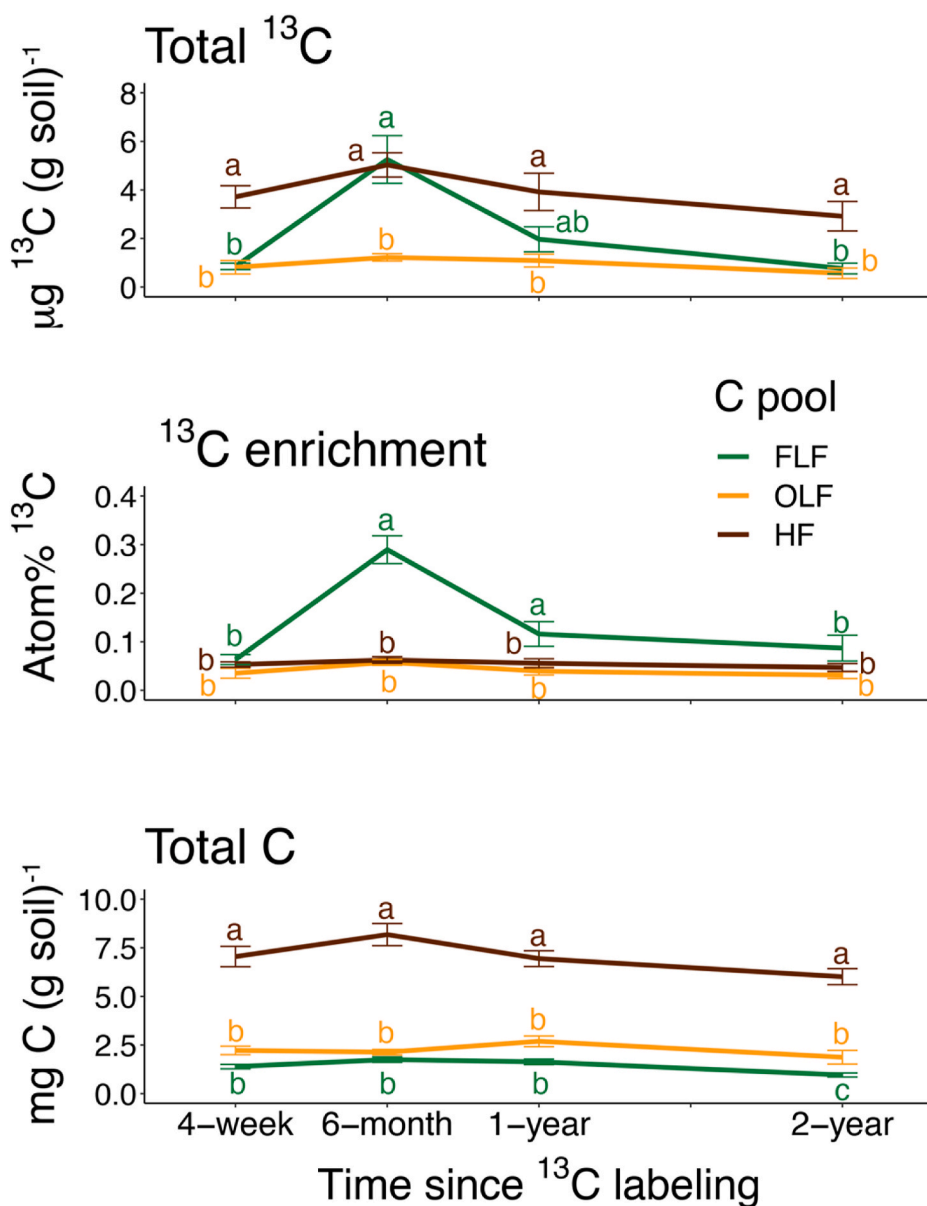


**Fig. 2.** Total  $^{13}\text{C}$ ,  $^{13}\text{C}$  enrichment, and total C distribution over time among soil density fractions after 5 days of *in situ*  $^{13}\text{CO}_2$  labelling. Total  $^{13}\text{C}$ ,  $^{13}\text{C}$  enrichment, and total C were measured for three soil density fractions: free-light fraction (FLF), occluded-light fraction (OLF), and heavy fraction (HF). Soil density fractions were determined on samples collected at 4-weeks, 6-months, 1-year, and 2-years post-labelling. Error bars represent 1 standard error ( $n = 8$ ). Different letters indicate significant differences among density fractions and sampling time ( $p < 0.05$ ). Letters referring to each density fraction are in the same color as the lines. Details of total  $^{13}\text{C}$  and total C results are presented in Table 2. (For interpretation of the references to color in this figure legend, the reader is referred to the Web version of this article.)

pattern to total C, but with an even greater proportion of N accumulating in the HF (Table 2): 83% in the HF, 10% in the OLF, and 7% in the FLF. The C:N ratio varied significantly by fraction type ( $p < 0.05$ ): highest in FLF (~20:1), intermediate in OLF (~18:1), and lowest in HF (~8:1). Total C, N, and C:N (Table 2, Fig. 2) did not exhibit detectable fluctuations between sampling times.

The  $^{13}\text{C}$  labeling event occurred during the growing season in February 2018, and samplings occurred 4 weeks, 6 months, 1 year, and 2 years later. Four weeks after the  $^{13}\text{C}$  labeling, 27% of the initial ecosystem  $^{13}\text{C}$  was recovered belowground. Of that, significantly more was recovered in the HF than in the OLF or FLF (Fig. 2). While accumulation of total C was higher in the OLF than FLF,  $^{13}\text{C}$  was slightly higher in the FLF than the OLF at the 4-week sample time.  $^{13}\text{C}$  enrichment (atom%  $^{13}\text{C}$ ) was significantly higher in the FLF than either the HF or OLF at 6 months (Fig. 2). Between the 4-week and 6-month sampling times, soil organic  $^{13}\text{C}$ -labeled C ( $\text{SO}^{13}\text{C}$ ) recovered in the density fractions roughly doubled, with the majority of additional  $\text{SO}^{13}\text{C}$  accumulating in the FLF (Fig. 2). At 6 months, the amount of  $^{13}\text{C}$  recovered in the FLF was similar to that in the HF. Between 6 months and 1 year after labeling,  $\text{SO}^{13}\text{C}$  content of the belowground samples declined from 64%

of the starting amount to 37%, with a particularly large decrease observed in FLF material. The 2-year  $^{13}\text{C}$  recovery in the soil density fractions was about half that recovered in the 1-year samples. By the 2-year sampling time, isotopically labeled C persisted in all three fractions, with over 80% of the remaining ecosystem  $^{13}\text{C}$  (representing 19% of the initial ecosystem  $^{13}\text{C}$  content) found in more protected forms, either occluded within soil microaggregates (OLF) or associated with soil minerals (HF) (Fig. 2).

### 3.3. $^{13}\text{C}$ NMR analysis of mineral-associated carbon

Heavy fraction (HF) material from 4-week, 1-year, and 2-year sampling times was analyzed by  $^{13}\text{C}$  NMR to assess the molecular forms taken by the newly fixed  $^{13}\text{C}$  and present in the HF. Likely due to the presence of paramagnetic minerals in these soils, the peaks in the  $^{13}\text{C}$  NMR spectra were somewhat broad and hence we were not able to identify specific compounds. Instead, we assessed relative proportions of broad chemical classes based on chemical shift regions in the NMR spectra: alkyl C 0–45 ppm, O-alkyl C 45–110 ppm, aromatic C 110–162 ppm, and carbonyl/carboxylic C 162–190 ppm (Fig. 3, Supplemental

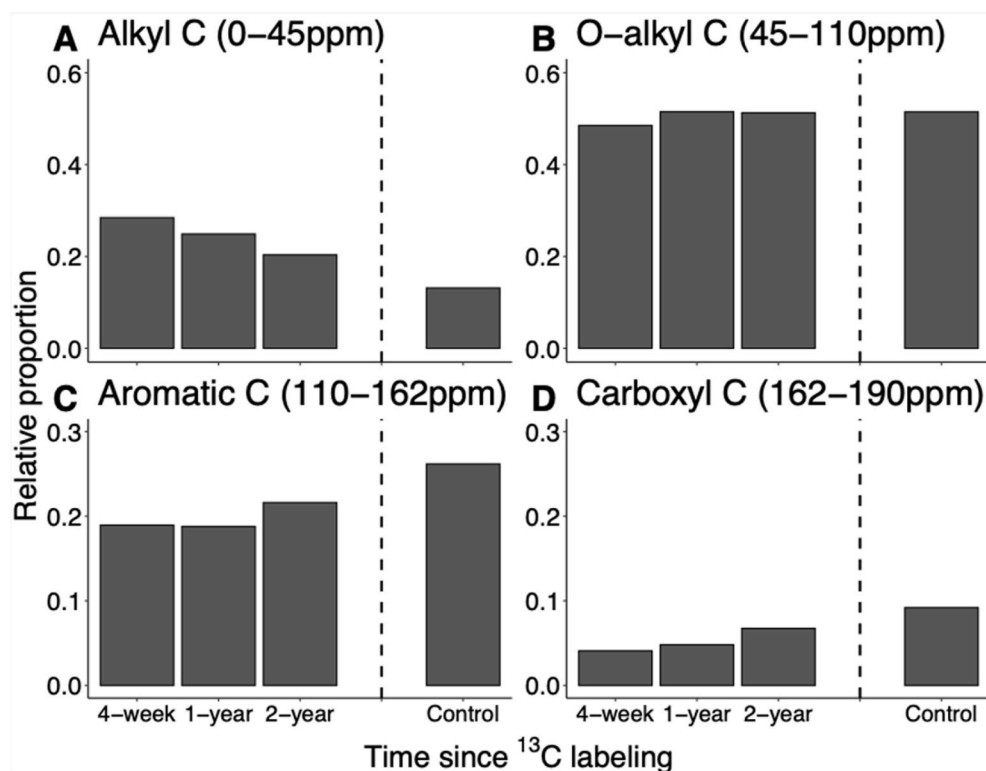


Fig. 3).

Labeling plants with  $^{13}\text{CO}_2$  allowed us to follow the functional group characteristics of newly fixed C incorporated into the mineral-associated pool (Fig. 3). The  $\text{SO}^{13}\text{C}$ -HF spectra was dominated by O-Alky, alkyl, and aromatic C with a smaller contribution of carboxylic. In the  $^{13}\text{C}$  NMR spectra, the relative proportion of alkyl C declined from 4 weeks to 1 year to 2 years after the  $^{13}\text{C}$  labeling. Over this same period, the relative proportion of aromatic and carboxyl C increased, while the relative proportion of O-alkyl C remained fairly constant. While the proportion of C functional groups in the  $^{13}\text{C}$ -labeled HF material was distinct from the  $^{12}\text{C}$ -labeled control HF material at all sampling times, the relative proportions of C functional groups in the  $^{13}\text{C}$ -labeled material appeared to become more similar to those observed in the control material over time (Fig. 3).

## 4. Discussion

### 4.1. Ecosystem $^{13}\text{C}$ incorporation

In this California annual grassland, allocation of aboveground photosynthate C to root growth is highest in late winter months (Feb–March) (Jackson et al., 1989). We targeted this time period for our February 2018, *in situ* 5-day  $^{13}\text{CO}_2$  field labeling experiment, designed to track the transfer of plant photosynthate into underground C pools. At the end of our 5-day labelling, 40% of plant-assimilated  $^{13}\text{C}$  had been allocated belowground (Fig. 1), indicating that the growing plants were rapidly moving a substantial proportion of photosynthate belowground. This value is consistent with literature values which suggest 20% or more of plant-fixed C is lost via exudation (Kuzyakov and Domanski 2000; Bais et al., 2006; Badri and Vivanco, 2009), and an additional 20% is allocated to root biomass (typical root: shoot ratio is 1:5 in *Avena* spp. (Gao et al., 2019).

By the 4-week sampling time, much of the belowground  $^{13}\text{C}$  was already recoverable in the HF + OLF, suggesting that the  $^{13}\text{C}$  exudates and rhizodeposits (sloughed root tip cells, root hairs) released by growing roots were already contributing to the soil's more protected

Fig. 3. Heavy fraction  $^{13}\text{C}$  functional groups measured by solid state  $^{13}\text{C}$  nuclear magnetic resonance (NMR). Relative proportions of four major carbon functional groups in HF materials separated from soil were calculated from  $^{13}\text{C}$  NMR spectra, by integrating functional group regions A. alkyl C, B. O-alkyl C, C. aromatic C, and D. carboxyl C using Topspin software, and analyzed separately for each spectrum. X axis refers to spectra obtained for  $^{13}\text{C}$ -labeled HF soil at 4-week, 1-year, and 2-year sampling times, as well as a  $^{12}\text{C}$ -labeled control sample collected at the 4-week sampling time. Atom percent  $^{13}\text{C}$  for the 4 samples (4-week, 1-year, 2-year, and control) was 1.145, 1.139, 1.133, and 1.076 respectively.

organic matter pools. We expect that  $^{13}\text{C}$  associated with the HF fraction also came from microbial utilization of root exudates or from root exudates directly. By the 6-month sampling time, the  $^{13}\text{C}$  recovery in the FLF peaked, indicating that the once-growing roots had senesced to become part of the FLF pool.

We found that total ecosystem  $^{13}\text{C}$  assimilated (above + belowground  $^{13}\text{C}$  content) at the 4-week sampling time was statistically indistinguishable from the belowground assimilated  $^{13}\text{C}$  at the 6-month sampling time. Root growth of annual grass species characteristic of these systems has been shown to decline by March (Jackson et al., 1989), suggesting that the  $^{13}\text{C}$  recovered in the belowground pool at the 4-week sampling time (mid-March) may have been primarily composed of structural plant root compounds. Additionally, soil respiration in California annual grasslands typically declines after early April (Eviner, 2001), as sources of labile C substrates dwindle, and soil moisture begins to decline. This could explain why we saw little evidence of late growing-season decomposition or loss of  $^{13}\text{C}$ .  $^{13}\text{C}$  recovery in the belowground pool at 6-months was 64% of the total  $^{13}\text{C}$  present immediately following the labeling. Other studies in California annual grassland ecosystems have described similarly high accumulations of C (Schaeffer et al., 2017), and added  $^{13}\text{C}$  (Castanha et al., 2018) over the summer dry period. This appears to occur because of the large C input as dead root litter (following annual plant senescence and death in May–July each year), and the reduced ability of microbes to access and decompose this C due to the very low soil moisture characteristic of the Mediterranean-type summer; desiccation results in very low activity of decomposers as well as physical isolation from C substrates (Blankinship and Schimel, 2018).

### 4.2. Soil density fractions

In our study, the vast majority of  $\text{SO}^{13}\text{C}$  was recovered in the HF pool. We assume the HF is primarily composed of mineral-associated organic matter (MAOM), i.e. organic matter stabilized via mineral sorption and co-precipitation mechanisms (Kögel-Knabner et al., 2008). Mineral-associated SOM generally has a C:N ratio that aligns with the C:

N ratio of microbes (~10), as opposed to living plant material (>20), (Clemente et al., 2011). In our study, the HF C:N ratio was consistently near 9:1, suggesting this C was largely of microbial origin (i.e. cellular residues of organisms that had assimilated plant C inputs) or reflected plant matter that had been preferentially mined of high C compounds. It has been shown that compared to plant-derived compounds, microbial products are more efficiently and effectively adsorbed to and stabilized by soil minerals (Lavallee et al., 2019). Furthermore, microbial transformation of detrital C inputs can be a critical precursor to long-term C stabilization (Cotrufo et al., 2013).

The C:N ratios of the FLF and OLF were respectively 20:1 and 17.5:1, reflecting a more plant-like composition than the HF material. California annual grasslands are typically dominated by annual herbaceous plant communities whose litter decomposes completely within two to three years (Eviner and Firestone, 2007), resulting in minimal FLF accumulation compared to other ecosystems (Crow et al., 2007). C-rich fungal hyphae, bacterial extracellular polysaccharides (EPS), and plant mucilage promote soil aggregation both as physical structuring agents as well as major contributors to aggregate-associated soil C (Six et al., 2004). In our soils, OLF material is largely dominated by fine root fragments and fungal hyphae (Kakouridis et al., 2021). The intermediate C:N ratio we measured in the OLF (between the FLF and HF) suggests that microbial residues and aggregation mechanisms such as fungal hyphae and bacterial EPS may have contributed to OLF formation in our samples. If we interpret C:N ratios as an indicator of decomposition, then our data suggests increasing decomposition progressing from FLF to OLF to HF (Hyvonen et al., 1996).

The characteristics of the  $^{13}\text{C}$  recovered in the density fractions likely differ by season.  $^{13}\text{C}$  recovered from 4-week soil may represent mostly rhizodeposits and labile C substrates exuded by roots and likely consumed by root-associated bacteria and fungi as well as AMF-mediated C flow from  $^{13}\text{CO}_2$ -labeled plants (Kakouridis et al., 2021). We observed a conspicuous increase in FLF  $^{13}\text{C}$  content between 4-weeks and 6-months due to rapid incorporation of  $^{13}\text{C}$ -labeled root detritus into this fraction following plant senescence and death, as well as likely incorporation of some aboveground litter. By our 6-month sampling, at the end of the summer dry period, much of the  $^{13}\text{C}$  in FLF would have been composed of senesced/dead root detritus; we assume that most of the  $^{13}\text{C}$  in the HF and OLF was initially root-derived and subsequently processed by microbes (Jackson et al., 2017). Between our 6-month and 1-year sampling, over half of the FLF  $^{13}\text{C}$  was lost, likely as either  $\text{CO}_2$  or DOC. The onset of rainfall from the 2018-2019 growing season likely triggered decomposition of senesced  $^{13}\text{C}$ -labeled plant biomass derived from the previous growing season. Some of this decomposing  $^{13}\text{C}$ -labeled material could also have been incorporated into the soil, representing an additional  $^{13}\text{C}$  source for HF and OLF pools measured at the 1-year sampling time.

Notably, we did not observe much seasonal transience in  $^{13}\text{C}$  enrichment in the OLF or HF. The spike of  $^{13}\text{C}$  in the FLF at 6-months after labeling did not appear to lead to an increase in OLF or HF  $^{13}\text{C}$  at subsequent time points. From our observations, the migration of  $^{13}\text{C}$  from root litter to FLF to HF appeared to be small. Instead, most of the mineral associated  $^{13}\text{C}$  that persisted over the two years appears to have entered the HF pool within 4 weeks after the field labeling and was derived primarily from exudates of living roots directly or indirectly via microbial processing. Similar conclusions have been recently reported in a greenhouse mesocosm study and  $^{13}\text{C}$  amendment studies (Neurath et al., 2021; Sokol et al., 2019a, 2019b). Our results provided *in situ* field evidence that MAOC primarily originates from root exudates regardless of the highly variable seasonal conditions.

Of the three fractions,  $^{13}\text{C}$  content was generally lowest in the OLF. This could suggest that the incorporation of 'new' C into soil aggregates occurs less rapidly than associations with minerals, or that stable aggregate formation requires repeated iterations of environmental fluctuations, such as annual plant growth periods or seasonal wet-dry cycles, which were not captured in the timespan of this study (Totsche

et al., 2017). However, over this two year study, the distribution of  $^{13}\text{C}$  among the density fractions approached the proportional distribution observed in the total SOC (highest amount in HF, followed by OLF, then FLF) (Fig. 2).

Our results indicate that associations between minerals and root-derived organic C form surprisingly rapidly. Rapid association of fresh root-derived C with mineral surfaces was also observed by Neurath et al. (2021), who characterized short-term dynamics (three months) of root-input C in a greenhouse study using similar soils. In that study, the flux of new root-derived C both onto and off of mineral surfaces was substantial (accounting for over 6% of total C), while total mineral-associated C remained constant. For our study, this implies that some of the  $^{13}\text{C}$ -HF associations could have been more dynamic than we were able to document. At four weeks after  $^{13}\text{C}$  labeling, we recovered 67% of soil  $^{13}\text{C}$  in the HF, and the quantity of  $^{13}\text{C}$  recovered in HF material did not detectably decline over the course of the study. By our two-year sampling, 77% of the initial  $^{13}\text{C}$  had been lost; of the  $^{13}\text{C}$  remaining, the majority (80%) was occluded within soil micro-aggregates or associated with soil minerals. These observations support the importance of root and rhizosphere-derived C inputs in SOM formation (Sokol and Bradford, 2019; Pett-Ridge and Firestone, 2017), and are consistent with rapid microbially-mediated association of C onto mineral surfaces (Kallenbach et al., 2016). However, they do not necessarily imply that rapidly created rhizosphere MAOM is persistent. While OLF and HF fractions sometimes contain SOC that is older (and presumed more persistent), recent work indicates mineral association does not have a universally protective function (Kleber et al., 2021; Li et al., 2021; Neurath et al., 2021; Keiluweit et al., 2015). Our NMR results suggest significant 'reworking' of the HF associated  $^{13}\text{C}$  occurred during two years of our study.

In this study, newly fixed SOC in the HF pool represented a significant portion of initial plant C inputs. While the majority of annual C inputs decomposed rapidly (<two year timescale), a sizeable proportion (~16%) of the original  $^{13}\text{C}$  inputs remained associated with the HF after two years and some of this SOC could potentially persist longer. In a study modeling soil C turnover in a California grassland site with similar physical characteristics, Torn et al. (2013) calculated that 7% of HF C sampled from the 1–15 cm depth was 'fast' cycling (<two year turnover) and 93% cycled on a centennial timescale. Our observations of rapid sorption and then evolving chemical composition (NMR data) provide some support for the existence of this rapidly cycling HF C pool, but also suggest that the HF does not represent a single C pool operating on a single timescale, but rather multiple pools operating on multiple timescales (Lehmann and Kleber, 2015; Sierra et al., 2018).

Because most agricultural and grassland soils are not accruing SOC (Sanderman et al., 2017), we originally predicted that newly added plant  $^{13}\text{C}$  would decline to negligible levels by the end of two years. Instead, a significant portion of the initial C input was retained (23% overall; 16% in the HF), while overall SOC levels remained static. This suggests priming, erosion, and DOC leaching must have also occurred to counterbalance the input of new SOC. With the dramatic decrease in the amount of California annual grasslands from over 10 million ha in 1992 (Heady et al., 1992) to just over 2.8 million ha in 2020 (George 2020), conservation of the remaining area and management of SOC is important due to grasslands' potential for long term C storage in the HF.

#### 4.3. $^{13}\text{C}$ NMR of mineral associated organic carbon

By applying  $^{13}\text{C}$  CPMAS NMR spectroscopy to our  $^{13}\text{C}$  labeled HF samples, we sought to resolve the chemical fingerprint of 'new' plant-derived C involved in MAOM. In the two-years post labelling, molecular characteristics of the  $^{13}\text{C}$  HF evolved (Fig. 3); the proportion of  $^{13}\text{C}$  in the alkyl C functional group declined, while the amount in the aromatic C and carboxyl C functional groups increased. As these chemical transformations occurred, we expect that only the most persistent  $^{13}\text{C}$ -HF associations were retained. This remaining C reflects the legacy of plant-

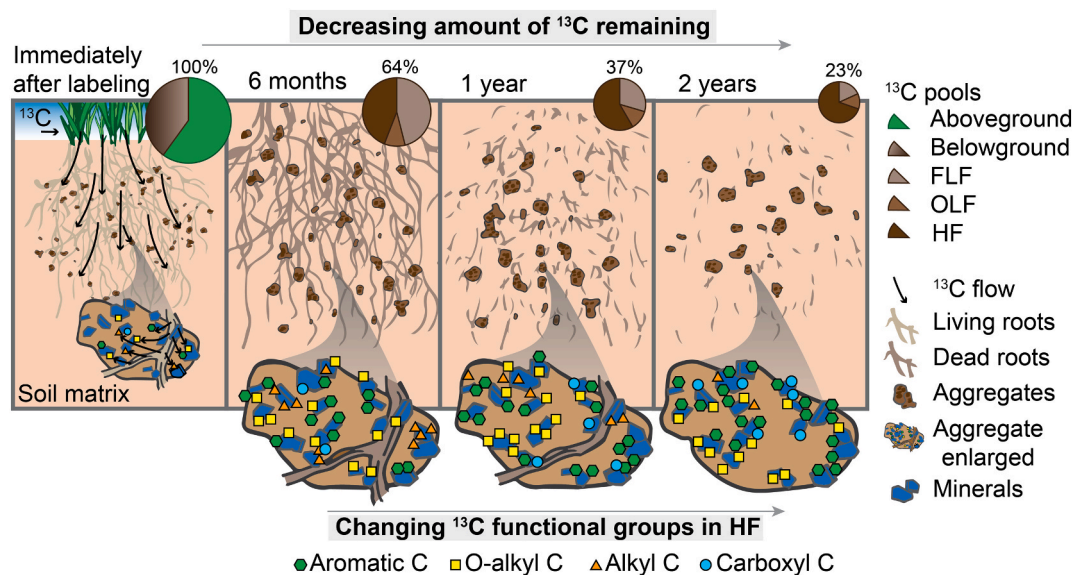


**Fig. 4.** Conceptual figure showing the flow and fate of  $^{13}\text{C}$  following a 5-day  $^{13}\text{CO}_2$  labeling in an annual grassland soil. Panels from left to right show sampling times (0-day, 6-month, 1-year, and 2-year). Over time, the amount of  $^{13}\text{C}$  remaining in the ecosystem decreased, as represented by the progressively smaller pie charts. The relative proportions of  $^{13}\text{C}$  in different C pools and soil density fractions changed over time, with less  $^{13}\text{C}$  recovered from FLF and more from HF. The  $^{13}\text{C}$  functional groups in the HF that associated with minerals changed in composition, with increased amount of aromatic and carboxyl C, and decreased amount of alkyl C.

added  $^{13}\text{C}$  that could persist for decades or even centuries (Baisden et al., 2002).

In  $^{13}\text{C}$  NMR spectra, the alkyl C functional group reflects a variety of microbial and plant-derived aliphatic compounds such as lipids, proteins, and waxes (Kögel-Knabner, 1997). Recent studies indicate that microbial products are a dominant source of mineral-stabilized organic matter that builds up in HF material over time (Preston et al., 2009; Creamer et al., 2019). Indeed, in HF material isolated from a similar soil, Neurath et al. found that mineral-associated lipids were largely microbially derived (Neurath et al., 2021). In our study, the relatively constant amount of  $^{13}\text{C}$  present in the HF yet declining alkyl  $^{13}\text{C}$  over two years suggests that alkyl  $^{13}\text{C}$  may have been oxidized to carboxyl  $^{13}\text{C}$ , or alternatively, that a portion of HF  $^{13}\text{C}$  is transient, and alkyl  $^{13}\text{C}$  was lost while carboxyl  $^{13}\text{C}$  preferentially accumulated. Regardless, the substantial alkyl  $^{13}\text{C}$  we measured shortly after the  $^{13}\text{CO}_2$  labeling suggests that rhizodeposition C is an important source of rapidly forming mineral-alkyl C associations, whether as plant waxes such as cutin, or microbial lipids as suggested by Neurath et al. (2021).

Peaks in the O-alkyl C region may represent various carbohydrates, proteins, and amino acids (Mathers et al., 2007), including plant-derived carbohydrates such as cellulose and hemicellulose (Kögel-Knabner, 1997), as well as N-rich proteins and root-exudate derived sugars (Angst et al., 2018). O-Alkyl C proportions in HF samples have also been attributed to carbohydrates of microbial origin (Schöning and Kögel-Knabner, 2006). In our study, the amount of HF O-alkyl C remained relatively constant after our *in situ* labeling, and was similar to background levels measured in unamended soils.

We measured an increase in both HF aromatic C and carboxyl C with time. The aromatic C functional group is thought to represent plant-derived phenolic compounds such as lignin and tannins, aromatic portions of proteins and amino acids, as well as condensed, chemically resistant “black carbon”. In our system, this could be derived from historically frequent wildfires that occurred in California annual grasslands (Sanderman et al., 2008; Czimczik and Maseillo, 2007). The carboxyl C functional group includes highly oxidized C forms such as organic acids, ketones, and aldehydes (Kögel-Knabner et al., 2008; Mathers et al., 2007), and can be used as an indicator of microbial processing (Ng et al., 2014). In our data, the increase in the relative proportion of carboxyl C

likely resulted from the oxidation of organic matter during the process of decomposition (Baldoek et al., 1992).

## 5. Conclusions and future directions

Understanding the patterns and drivers of SOC cycling in California annual grasslands is a critical precursor to soil management in these ecosystems. Using an *in situ*  $^{13}\text{C}$  labeling approach, we found a surprisingly large amount of plant-fixed C (23%) persists for multiple years after it enters the belowground system. Carbon released from roots rapidly associated with mineral surfaces, and after two years, this pool remained the largest sink for plant-derived C (Fig. 4). While the total  $^{13}\text{C}$  enrichment of the mineral associated pool was highly stable, NMR analysis showed the molecular fingerprint of these compounds evolved with time, with increased amounts of  $^{13}\text{C}$  aromatic and carboxyl C functional groups, and less alkyl C. This suggests both reworking and losses of HF-associated compounds.

Relatively few *in situ* studies have followed the amount of plant-fixed C that persists in soil over a period of multiple years. This approach is a powerful way to track whole-system flows of plant C from ‘cradle to grave’, in an intact, undisturbed manner. Future research that tracks C dynamics over decadal timescales can further resolve how plant community characteristics (plant growth stage, lifecycle, seasonal climate parameters) influence the accrual and persistence of SOC and help to better predict the responsiveness of annual grassland ecosystems to soil C management.

## Declaration of competing interest

The authors declare that they have no known competing financial interests or personal relationships that could have appeared to influence the work reported in this paper.

## Acknowledgements

This research was supported by the US Department of Energy (DOE) Office of Science, Office of Biological and Environmental Research Genomic Science program under awards DE-SC0020163 and DE-

SC0016247 (to MKF) and awards SCW1589, SCW1421 and the LLNL Soil Microbiome SFA, SCW1632 (to JPR). Work at Lawrence Livermore National Laboratory was conducted under the auspices of the U.S. DOE under Contract DE-AC52-07NA27344. Work conducted at Lawrence Berkeley National Laboratory was supported under Contract DE-AC02-05CH11231. Soil and plant collection and field plot management was supported by the Hopland Research and Extension Center through the University of California Division of Agriculture and Natural Resources.

## Appendix A. Supplementary data

Supplementary data to this article can be found online at <https://doi.org/10.1016/j.soilbio.2021.108519>.

## References

- Angst, G., Messinger, J., Greiner, M., Häusler, W., Hertel, D., Kirfel, K., et al., 2018. Soil organic carbon stocks in topsoil and subsoil controlled by parent material, carbon input in the rhizosphere, and microbial-derived compounds. *Soil Biology and Biochemistry* 122, 19–30. <https://doi.org/10.1016/j.soilbio.2018.03.026>.
- Angst, G., Mueller, K.E., Klass, G.J.N., Simpson, M.J., 2021. Plant- or microbial-derived? A review on the molecular composition of stabilized soil organic matter. *Soil Biology and Biochemistry* 156. <https://doi.org/10.1016/j.soilbio.2021.108189>.
- AOAC Official method 972.43, microchemical determination of carbon, hydrogen, and nitrogen, automated method. In: *Official Methods of Analysis of AOAC International*, sixteenth ed., 1997. AOAC International, Arlington, VA, pp. 5–6 (Chapter 12).
- Badri, D.V., Vivanco, J.M., 2009. Regulation and function of root exudates. *Plant, Cell and Environment* 32 (6), 666–681.
- Bailey, V.L., Pries, C.H., Lajtha, K., 2019. What do we know about soil carbon destabilization? *Environmental Research Letters* 14 (8), 083004. <https://doi.org/10.1088/1748-9326/ab2c11>.
- Bais, H.P., Weir, T.L., Perry, L.G., Gilroy, S., Vivanco, J.M., 2006. The role of root exudates in rhizosphere interactions with plants and other organisms. *Annual Review of Plant Biology* 57, 233–266.
- Baker, S.E., Peridas, G., Stolaroff, J.K., Goldstein, H.M., Pang, S.H., Lucci, F.R., Li, W., Slessarev, E.W., Pett-Ridge, J., Ryerson, F.R., Aines, R.D., 2019. Getting to Neutral: Options for Negative Carbon Emissions in California (No. LLNL-TR-796100). Lawrence Livermore National Laboratory (LLNL), Livermore, CA (United States).
- Baisden, W.T., Amundson, R., Cook, A.C., Brenner, D.L., 2002. Turnover and storage of C and N in five density fractions from California annual grassland surface soils. *Global Biogeochemical Cycles* 16 (4), 64–71. <https://doi.org/10.1029/2001gb001822>.
- Bakker, E., Hubert, F., Wander, M.M., Lanson, B., 2018. Soil development under continuous agriculture at the morrow plots experimental fields from X-ray diffraction profile modelling. *Soil System* 2, 46. <https://doi.org/10.3390/soilsystems2030046>.
- Baldock, J.A., Oades, J.M., Waters, A.G., Peng, X., Vassallo, A.M., Wilson, M.A., 1992. Aspects of the chemical structure of soil organic materials as revealed by solid-state  $^{13}\text{C}$  NMR spectroscopy. *Biogeochemistry* 16 (1), 1–42.
- Barnard, R., Blazewicz, S., Firestone, M., 2020. Rewetting of soil: revisiting the origin of soil CO<sub>2</sub> emissions. *Soil Biology and Biochemistry*. <https://doi.org/10.1016/j.soilbio.2020.107819>.
- Bartolome, J.W., Barry, J., Griggs, T., Hopkinson, P., 2007. Valley grasslands. In: *Barbour, M.G., Keeler-Wolf, T., Schoenherr, A.A. (Eds.), Terrestrial Vegetation of California*. University of California Press, Berkeley, California, pp. 367–393.
- Biggs, N.B., Huntsinger, L., 2021. Managed grazing on California annual rangelands in the context of state climate policy. *Rangeland Ecology & Management* 76 (1), 56–68. <https://doi.org/10.1016/j.rama.2021.01.007>.
- Blankinship, J., Schimel, J., 2018. Biotic versus abiotic controls on bioavailable soil organic carbon. *Soil Systems* 2 (1), 10. <https://doi.org/10.3390/soilsystems2010010>.
- Bradford, M.A., Carey, C.J., Atwood, L., Bossio, D., Fenichel, E.P., Gennet, S., et al., 2019. Soil carbon science for policy and practice. *Nature Sustainability* 2 (12), 1070–1072. <https://doi.org/10.1038/s41893-019-0431-y>.
- Castanha, C., Zhu, B., Hicks Pries, C.E., Georgiou, K., Torn, M.S., 2018. The effects of heating, rhizosphere, and depth on root litter decomposition are mediated by soil moisture. *Biogeochemistry* 137 (1), 267–279. <https://doi.org/10.1007/s10533-017-0418-6>.
- Clemente, J.S., Simpson, A.J., Simpson, M.J., 2011. Association of specific organic matter compounds in size fractions of soils under different environmental controls. *Organic Geochemistry* 42 (10), 1169–1180. <https://doi.org/10.1016/j.orggeochem.2011.08.010>.
- Cotrufo, M.F., Wallenstein, M.D., Boot, C.M., Deneff, K., Paul, E., 2013. The Microbial Efficiency-Matrix Stabilization (MEMS) framework integrates plant litter decomposition with soil organic matter stabilization: do labile plant inputs form stable soil organic matter? *Global Change Biology* 19 (4), 988–995. <https://doi.org/10.1111/gcb.12113>.
- Cotrufo, M.F., Soong, J.L., Horton, A.J., Campbell, E.E., Haddix, M.L., Wall, D.H., Parton, W.J., 2015. Formation of soil organic matter via biochemical and physical pathways of litter mass lost. *Nature Geoscience* 8 (10), 776–779. <https://doi.org/10.1038/ngeo2520>.
- Cotrufo, M.F., Ranalli, M.G., Haddix, M.L., Six, J., Lugato, E., 2019. Soil carbon storage informed by particulate and mineral-associated organic matter. *Nature Geoscience* 12 (12), 989–994. <https://doi.org/10.1038/s41561-019-0484-6>.
- Creamer, C.A., Foster, A.L., Lawrence, C., McFarland, J., Schulz, M., Waldrop, M.P., 2019. Mineralogy dictates the initial mechanism of microbial necromass association. *Geochimica et Cosmochimica Acta* 260, 161–176. <https://doi.org/10.1016/j.gca.2019.06.028>.
- Crow, S.E., Swanston, C.W., Lajtha, K., Brooks, J.R., Keirstead, H., 2007. Density fractionation of forest soils: methodological questions and interpretation of incubation results and turnover time in an ecosystem context. *Biogeochemistry* 85, 69–90. <https://doi.org/10.1007/s10533-007-9100-8>.
- Cusack, D.F., Halterman, S.M., Tanner, E.V.J., Wright, S.J., Hockaday, W., Diatterich, L.H., Turner, B.L., 2018. Decadal-scale litter manipulation alters the biochemical and physical character of tropical forest soil carbon. *Soil Biology and Biochemistry* 124, 199–209. <https://doi.org/10.1016/j.soilbio.2018.06.005>.
- Czimczik, C.I., Maseillo, C.A., 2007. *Global Biogeochemical Cycles* 21 (1), GB3005. <https://doi.org/10.1029/2006GB002798>.
- Dass, P., Houlton, B.Z., Wang, Y., Warlind, D., 2018. Grasslands may be more resilient carbon sinks than forests in California. *Environmental Research Letters* 13 (7). <https://doi.org/10.1088/1748-9326/aacb39>.
- Doebelin, N., Kleeberg, R., 2015. Profex: a graphical user interface for the Rietveld refinement program BGMN. *Journal of Applied Crystallography* 48, 1573–1580.
- Eviner, V., 2001. Linking trait community composition and ecosystem dynamics: interactions of plant traits determine the ecosystem effects of plant species and plant species mixtures. PhD Dissertation. Integrative Biology. The University of California, Berkeley, p. 404.
- Eviner, V.T., Firestone, M.K., 2007. In: *Stromberg, M., Corbin, J., D'Antonio, C. (Eds.), Mechanisms Determining Patterns of Nutrient Dynamics, California Grasslands: Ecology and Management*. University of California Press, Berkeley, California, pp. 94–106.
- Gao, K., Yu, Y.F., Xia, Z.T., Yang, G., Xing, Z.L., Qi, L.T., Ling, L.Z., 2019. Response of height, dry matter accumulation and partitioning of oat (*Avena sativa* L.) to planting density and nitrogen in Horqin Sandy Land. *Scientific Reports* 9 (1), 1–7.
- George, M., 2020. *Ecology and Management of Annual Rangelands Series: Mediterranean Climate*. Retrieved from. <https://escholarship.uc/item/9sd638zh>.
- Geyer, K., Schneckner, J., Grandy, A.S., Richter, A., Frey, S., 2020. Assessing microbial residues in soil as a potential carbon sink and moderator of carbon use efficiency. *Biogeochemistry* 151 (2), 237–249.
- Golchin, A., Oades, J., Skjemstad, J., Clarke, P., 1994. Study of free and occluded particulate organic matter in soils by solid state  $^{13}\text{C}$  CP/MAS NMR spectroscopy and scanning electron microscopy. *Soil Research* 32, 285–309. <https://doi.org/10.1071/SR9940285>.
- Heady, H.F., Bartolome, J.W., Pitt, M.D., Savelle, G.D., Stroud, M.C., 1992. California prairie. In: *Coupland, R.T. (Ed.), Natural Grasslands. Ecosystems of the World 8A*. Elsevier, New York, New York, pp. 313–335.
- Heckman, K.A., Swanston, C.W., Torn, M.S., Hanson, P.J., Nave, L.E., Porras, R.C., Mishra, U., Bill, M., 2021. Soil organic matter is principally root derived in an Ultisol under oak forest. *Geoderma* 403, 115385.
- Helfrich, M., Ludwig, B., Buurman, P., Flessa, H., 2006. Effect of land use on the composition of soil organic matter in density and aggregate fractions as revealed by solid-state  $^{13}\text{C}$  NMR spectroscopy. *Geoderma* 136 (1–2), 331–341. <https://doi.org/10.1016/j.geoderma.2006.03.048>.
- Hicks Pries, C.E., Bird, J.A., Castanha, C., Hatton, P.-J., Torn, M.S., 2017. Long term decomposition: the influence of litter type and soil horizon on retention of plant carbon and nitrogen in soils. *Biogeochemistry* 134 (1–2), 5–16. <https://doi.org/10.1007/s10533-017-0345-6>.
- Hicks Pries, C.E., Bird, J.A., Castanha, C., Hatton, P.J., Torn, M.S., 2017. Long term decomposition: the influence of litter type and soil horizon on retention of plant carbon and nitrogen in soils. *Biogeochemistry* 134 (1), 5–16.
- Hyvonen, R., Agren, G.I., Andren, O., 1996. Modelling long-term carbon and nitrogen dynamics in an arable soil receiving organic matter. *Ecological Applications* 6 (4), 1345–1354. <https://doi.org/10.2307/2269612>.
- Jackson, L.E., Schimel, J.P., Firestone, M.K., 1989. Short-term partitioning of ammonium and nitrate between plants and microbes in an annual grassland. *Soil Biology and Biochemistry* 21 (3), 409–415. [https://doi.org/10.1016/0038-0717\(89\)90152-1](https://doi.org/10.1016/0038-0717(89)90152-1).
- Jackson, R.B., Lajtha, K., Crow, S.E., Hugelius, G., Kramer, M.G., Pineiro, G., 2017. The ecology of soil carbon: pools, vulnerabilities, and biotic and abiotic controls. *Annual Review of Ecology, Evolution and Systematics* 48 (1), 419–445. <https://doi.org/10.1146/annurev-ecolsys-112414-054234>.
- Kakouridis, A., Yuan, M., Hagen, J., Fossium, C., Moore, M., Herman, D., Nico, P., Weber, P., Pett-Ridge, J., Firestone, M.K., 2021. AMF transport of plant carbon into soil alters the characteristics of soil organic carbon as well as the soil microbial community. *bioRxiv*. <https://doi.org/10.1101/2020.09.21.305409>.
- Kallenbach, C.M., Frey, S.D., Grandy, A.S., 2016. Direct evidence for microbial-derived soil organic matter formation and its ecophysiological controls. *Nature Communications* 7 (1). <https://doi.org/10.1038/ncomms13630>.
- Kandeler, E., Gebala, A., Boeddinghaus, R.S., Müller, K., Rennett, T., Soares, M., Rousk, J., Marhan, S., 2019. The mineralosphere—Succession and physiology of bacteria and fungi colonising pristine minerals in grassland soils under different land-use intensities. *Soil Biology and Biochemistry* 136, 107534.
- Keiluweit, M., Bougoure, J.J., Nico, P.S., Pett-Ridge, J., Weber, P.K., Kleber, M., 2015. Mineral protection of soil carbon counteracted by root exudates. *Nature Climate Change* 5, 588–595.
- Kleber, M., Bourg, I.C., Coward, E.K., Hansel, C.M., Myneni, S.G., Nunan, N., 2021. Dynamic interactions at the mineral–organic matter interface. *Nature Reviews Earth & Environment* 2 (6), 402–421.

- Kögel-Knabner, I., 1997.  $^{13}\text{C}$  and  $^{15}\text{N}$  NMR spectroscopy as a tool in soil organic matter studies. *Geoderma* 80 (1), 243–260.
- Kögel-Knabner, I., Guggenberger, G., Kleber, M., Kandeler, E., Kalbitz, K., Scheu, S., Eusterhues, K., Leinweber, P., 2008. Organo-mineral associations in temperate soils: integrating biology, mineralogy, and organic matter chemistry. *Journal of Plant Nutrition and Soil Science* 171 (1), 61–82. <https://doi.org/10.1002/jpln.200700048>.
- Kuzyakov, Y., Domanski, G., 2000. Carbon input by plants into the soil. *Review. Journal of Plant Nutrition and Soil Science* 163 (4), 421–431.
- Lang, S.Q., Bernasconi, S.M., Früh-Green, G.L., 2012. Stable isotope analysis of organic carbon in small ( $\mu\text{g C}$ ) samples and dissolved organic matter using a GasBench preparation device. *Rapid Communications in Mass Spectrometry* 26 (1), 9–16. <https://doi.org/10.1002/rcm.5287>.
- Lavallee, J.M., Soong, J.L., Cotrufo, M.F., 2019. Conceptualizing soil organic matter into particulate and mineral-associated forms to address global change in the 21st century. *Global Change Biology* 26 (1), 261–273. <https://doi.org/10.1111/gcb.14859>.
- Lehmann, J., Kleber, M., 2015. The contentious nature of soil organic matter. *Nature* 528 (7580), 60–68. <https://doi.org/10.1038/nature16069>.
- Li, H., Bölscher, T., Winnick, M., Tfaily, M.M., Cardon, Z.G., Keiluweit, M., 2021. Simple plant and microbial exudates destabilize mineral-associated organic matter via multiple pathways. *Environmental Science and Technology* 55 (5), 3389–3398. <https://doi.org/10.1021/acs.est.0c04592>.
- Mathers, N.J., Jalota, R.K., Dalal, R.C., Boyd, S.E., 2007.  $^{13}\text{C}$ -NMR analysis of decomposing litter and fine roots in the semi-arid Mulga Lands of southern Queensland. *Soil Biology and Biochemistry* 39 (1), 993–1006. <https://doi.org/10.1016/j.soilbio.2006.11.009>.
- Mendiburu, F.D., 2015. *Agricolae: Statistical Procedures for Agricultural Research*, Version 1.2- 3. <http://CRAN.R-project.org/package=agricolae>.
- Neurath, R., Pett-Ridge, J., Chu-Jacoby, I., Herman, D., Whitman, T., Nico, P., Lipton, A. S., Kyle, J., Tfaily, M.M., Thompson, A., Firestone, M.K., 2021. Root carbon interaction with soil minerals is dynamic, leaving a legacy of microbially-derived residues. *Environmental Science and Technology* (19), 13345–13355. <https://doi.org/10.1021/acs.est.1c00300>.
- Ng, E.-L., Patti, A.F., Rose, M.T., Schefe, C.R., Wilkinson, K., Smernik, R.J., Cavanaugh, T. R., 2014. Does the chemical nature of soil organic carbon drive the structure and functioning of soil microbial communities? *Soil Biology and Biochemistry* 70 (1), 54–61. <https://doi.org/10.1016/j.soilbio.2013.12.004>.
- Pett-Ridge, J., Firestone, M.K., 2017. Using stable isotopes to explore root-microbe-mineral interactions in soil. *Rhizosphere* 3, 244–253. <https://doi.org/10.1016/j.rhisph.2017.04.016>.
- Pett-Ridge, J., Shi, J., Estera-Molina, K., Nuccio, E.E., Yuan, M., Rijkers, R., Swenson, T., Zhalnina, K., Northern, T., Zhou, J., Firestone, M.K., 2021. Rhizosphere carbon turnover from cradle to grave: the role of microbe-plant interactions. In: Gupta, V., Sharma, A. (Eds.), *Rhizosphere Biology: Interactions between Microbes and Plants*. Rhizosphere Biology. Springer, Singapore. [https://doi.org/10.1007/978-981-15-6125-2\\_2](https://doi.org/10.1007/978-981-15-6125-2_2).
- Poelau, C., Don, A., Six, J., Kaiser, M., Benbi, D., Chenu, C., Nieder, R., 2018. Isolating organic carbon fractions with varying turnover rates in temperate agricultural soils – a comprehensive method comparison. *Soil Biology and Biochemistry* 125, 10–26. <https://doi.org/10.1016/j.soilbio.2018.06.025>.
- Preston, C.M., Nault, J.R., Trofymow, J.A., 2009. Chemical changes during 6 years of decomposition of 11 litter in some Canadian forest sites. Part 2.  $^{13}\text{C}$  abundance, solid-state  $^{13}\text{C}$  NMR spectroscopy and the meaning of “lignin”. *Ecosystems* 12 (1), 1078–1102. <https://doi.org/10.1007/s10021-009-9267-z>.
- Sanderman, J., Baldock, J.A., Amundson, R., 2008. Dissolved organic carbon chemistry and dynamics in contrasting forest and grassland soils. *Biogeochemistry* 89 (2), 181–198.
- Sanderman, J., Hengl, T., Fiske, G.J., 2017. Soil carbon debt of 12,000 years of human land use. *Proceedings of the National Academy of Sciences* 114 (36), 9575–9580.
- Schaeffer, S.M., Homyak, P.M., Boot, C.M., Roux-Michollet, D., Schimel, J.P., 2017. Soil carbon and nitrogen dynamics throughout the summer drought in a California annual grassland. *Soil Biology and Biochemistry* 115, 54–62. <https://doi.org/10.1016/j.soilbio.2017.08.009>.
- Schöning, I., Kögel-Knabner, I., 2006. Chemical composition of young and old carbon pools throughout Cambisol and Luvisol profiles under forests. *Soil Biology and Biochemistry* 38 (1), 2411–2424. <https://doi.org/10.1016/j.soilbio.2006.03.005>.
- Sheldrick, B.H., Wang, C., 1993. Particle-size distribution. In: Carter, M.R. (Ed.), *Soil Sampling and Methods of Analysis*, Canadian Society of Soil Science. Lewis Publishers, Ann Arbor, MI, pp. 499–511.
- Sher, Y., Baker, N.R., Herman, D., Fossum, C., Hale, L., Zhang, X., et al., 2020. Microbial extracellular polysaccharide production and aggregate stability controlled by switchgrass (*Panicum virgatum*) root biomass and soil water potential. *Soil Biology and Biochemistry* 143, 107742. <https://doi.org/10.1016/j.soilbio.2020.107742>.
- Sierra, C.A., Hoyt, A.M., He, Y., Trumbore, S.E., 2018. Soil organic matter persistence as a stochastic process: age and transit time distributions of carbon in soils. *Global Biogeochemical Cycles* 32 (10), 1574–1588.
- Singer, M.J., Southard, R.J., Warrington, D.N., Janitzky, P., 1992. Stability of synthetic sand-clay aggregates after wetting and drying cycles. *Soil Science Society of America Journal* 56 (6), 1843–1848. <https://doi.org/10.2136/sssaj1992.0361599500560060032x>.
- Six, J., Bossuyt, H., Degryze, S., Denef, K., 2004. A history of research on the link between (micro)aggregates, soil biota, and soil organic matter dynamics. *Soil and Tillage Research* 79 (1), 7–31. <https://doi.org/10.1016/j.still.2004.03.008>.
- Sokol, N.W., Sanderman, J., Bradford, M.A., 2019a. Pathways of mineral-associated soil organic matter formation: integrating the role of plant carbon source, chemistry, and point of entry. *Global Change Biology* 25 (1), 12–24. <https://doi.org/10.1111/gcb.14482>.
- Sokol, N.W., Kuebbing, S.E., Karlsen-Ayala, E., Bradford, M.A., 2019b. Evidence for the primacy of living root inputs, not root or shoot litter, in forming soil organic carbon. *New Phytologist* 221 (1), 233–246.
- Sokol, N.W., Bradford, M.A., 2019. Microbial formation of stable soil carbon is more efficient from belowground than aboveground input. *Nature Geoscience* 12 (1), 46–53. <https://doi.org/10.1038/s41561-018-0258-6>.
- Sollins, P., Kramer, M.G., Swanston, C., Lajtha, K., Filley, T., Aufdenkampe, A.K., et al., 2009. Sequential density fractionation across soils of contrasting mineralogy: evidence for both microbial- and mineral-controlled soil organic matter stabilization. *Biogeochemistry* 96 (1–3), 209–231. <https://doi.org/10.1007/s10533-009-9359-z>.
- Strickland, T.C., Sollins, P., 1987. Improved method for separating light- and heavy-fraction organic material from soil. *Soil Science Society of America Journal* 51 (5), 1390–1393. <https://doi.org/10.2136/sssaj1987.03615995005100050056x>.
- Torn, M.S., Trumbore, S.E., Chadwick, O.A., Vitousek, P.M., Hendricks, D.M., 1997. Mineral control of soil organic carbon storage and turnover. *Nature* 389 (6647), 170–173. <https://doi.org/10.1038/38260>.
- Torn, M.S., Kleber, M., Zavaleta, E.S., Zhu, B., Field, C.B., Trumbore, S.E., 2013. A dual isotope approach to isolate soil carbon pools of different turnover times. *Biogeochemistry* 10 (1), 8067–8081. <https://doi.org/10.5194/bg-10-8067-2013>.
- Totsche, K.U., Amelung, W., Gerzabek, M.H., Guggenberger, G., Klump, E., Knief, C., et al., 2017. Microaggregates in soils. *Journal of Plant Nutrition and Soil Science* 181 (1), 104–136. <https://doi.org/10.1002/jpln.201600451>.
- Villarino, S.H., Pinto, P., Jackson, R.B., Piñeiro, G., 2021. Plant rhizodeposition: a key factor for soil organic matter formation in stable fractions. *Science Advances* 7 (16), 1–13. <https://doi.org/10.1126/sciadv.abd3176>.
- Wickham, H., 2016. *ggplot2: Elegant Graphics for Data Analysis*. Springer-Verlag, New York, ISBN 978-3-319-24277-4. <https://ggplot2.tidyverse.org>.
- Zhou, X., Liu, D., Bu, H., Deng, L., Liu, H., Yuan, P., Du, P., Song, H., 2018. XRD-based quantitative analysis of clay minerals using reference intensity ratios, mineral intensity factors, Rietveld, and full pattern summation methods: a critical review. *Solid Earth Sciences* 3, 16–29. <https://doi.org/10.1016/j.sesci.2017.12.002>.
- Zhu, X., Pei, Y., Zheng, Z., Dong, J., Zhang, Y., Wang, J., Chen, L., Doughty, R., Zhang, G., Xiao, X., 2018. Underestimates of grassland gross primary production in MODIS standard products. *Remote Sensing* 10 (11), 1771.